ACS APPLIED MATERIALS & INTERFACES

Research Article

www.acsami.org

Superparamagnetic Microspheres with Controlled Macroporosity Generated in Microfluidic Devices

Chantal Paquet,* Zygmunt J. Jakubek, and Benoit Simard*

Emerging Technologies Division, National Research Council, 100 Sussex Drive, Ottawa, Ontario K1A 0R6, Canada

Supporting Information

ABSTRACT: A microfluidic approach to preparing superparamagnetic microspheres with tunable porosity is described. In this method, droplets consisting of iron oxide nanoparticles, a functional polymer and solvent are formed in a microfluidic channel. The droplets are subsequently collected in solutions of sodium dodecyl sulfate (SDS) where the solvent is left to diffuse out of the droplet phase. By adjusting the concentration of the SDS and the polarity of the solvent of the dispersed phase, the porosity of the microparticles is controlled from non porous to porous structure. The formation of the pores is shown to depend on the rate at which solvent diffuses out of the droplet phase and the availability of SDS to adsorb at the droplet interface.

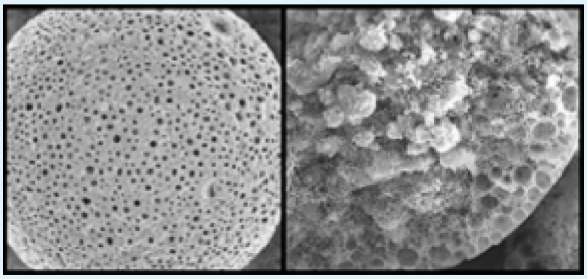

KEYWORDS: *microfluidic, superparamagnetic, porous, microparticles, assembly, magnetic separation*

1. INTRODUCTION

Microfluidic devices are being increasingly used as tools to synthesize a wide variety of particles, such as capsules, janus, double- or triple-emulsion, disks, rods, and porous particles.[1−9] This approach uses the shear force of one flowing fluid to break-up the flow of a second immiscible fluid into droplets.[10] Since the flow of the fluids can be finely adjusted, this method offers the advantages of precise control over the size of the droplets and produces narrow size distributions. The droplets, generally consisting of precursor materials such as monomer, prepolymer or metal alkoxides, are subsequently solidified into particles within the microchannel.[1,6,11] As the channel is normally limited in length, the conversion step must occur rapidly using efficient processes, such as photopolymerization or photo-cross-linking.[12,13] A problem thus arises if the precursor material is not amenable to rapid conversion, e.g., when the precursor materials are strongly light absorbing, or light- and heat-sensitive. Therefore, a method of preparing particles in microfluidic devices that is suitable for preparing microparticles of various morphologies from material that are difficult to solidify is required.

Porous materials find use in a wide range of applications including stationary phases in separation science, energy storage, sensors and membranes. Materials with interconnected and well-defined meso- (2−50 nm) and macropores (>50 nm) are particularly useful for applications that involve large molecules or viscous material due to enhanced diffusion rates inside large pores and the associated enhanced activity of the pores to reactants.[14] Porous particles have the benefits over monolith materials in the simplicity of packing them for applications using columns and the ease of handling them during extraction and purifications steps.[15] Porous particles with superparamagnetic properties offer the added advantage of being able to manipulate the particles with an external magnetic field, thus greatly simplifying the separation and washing of the particles from complex mixtures.[16−18] Furthermore, superparamagnetic particles that have well-defined structures and sizes can be sorted on the basis of the size and magnetic susceptibility of the particles in miniaturized on-chip systems using their magnetophoretic mobilities.[19]

Porous particles are generally synthesized using heteropolymerization schemes with porogens or as double emulsions.[15] Recently many of these techniques traditionally used to prepared porous particles have been adopted to work in microfluidic channels yielding particles with better control over their size and size distributions.[1,20−25] For instance, Kumacheva et al. have formed porous particles starting from droplets composed of a porogen and monomer.[21] The pores developed as the monomer photopolymerized in situ inducing phase separation with the porogen. Postpolymerization, the porogen was washed out to yield pores. The pore size was controlled by varying the solubility of the porogen in the monomer. Alternatively, highly porous polymer particles were formed from droplets made from a high internal phase emulsion (HIPE).[24] The oil of this water-in-oil emulsion consisted of monomer, which was photopolymerized within the channel to generate particles with large open cellular pores. In another example, monodispersed porous particles were formed by photopolymerizing an air-in-water-in-oil emulsion.[25] The triple component emulsion was formed by first producing air bubbles in an aqueous acrylamide solution followed by breaking the air-in-water emulsion at a T-junction with an oil phase.

Received: July 11, 2012
Accepted: August 17, 2012
Published: August 17, 2012

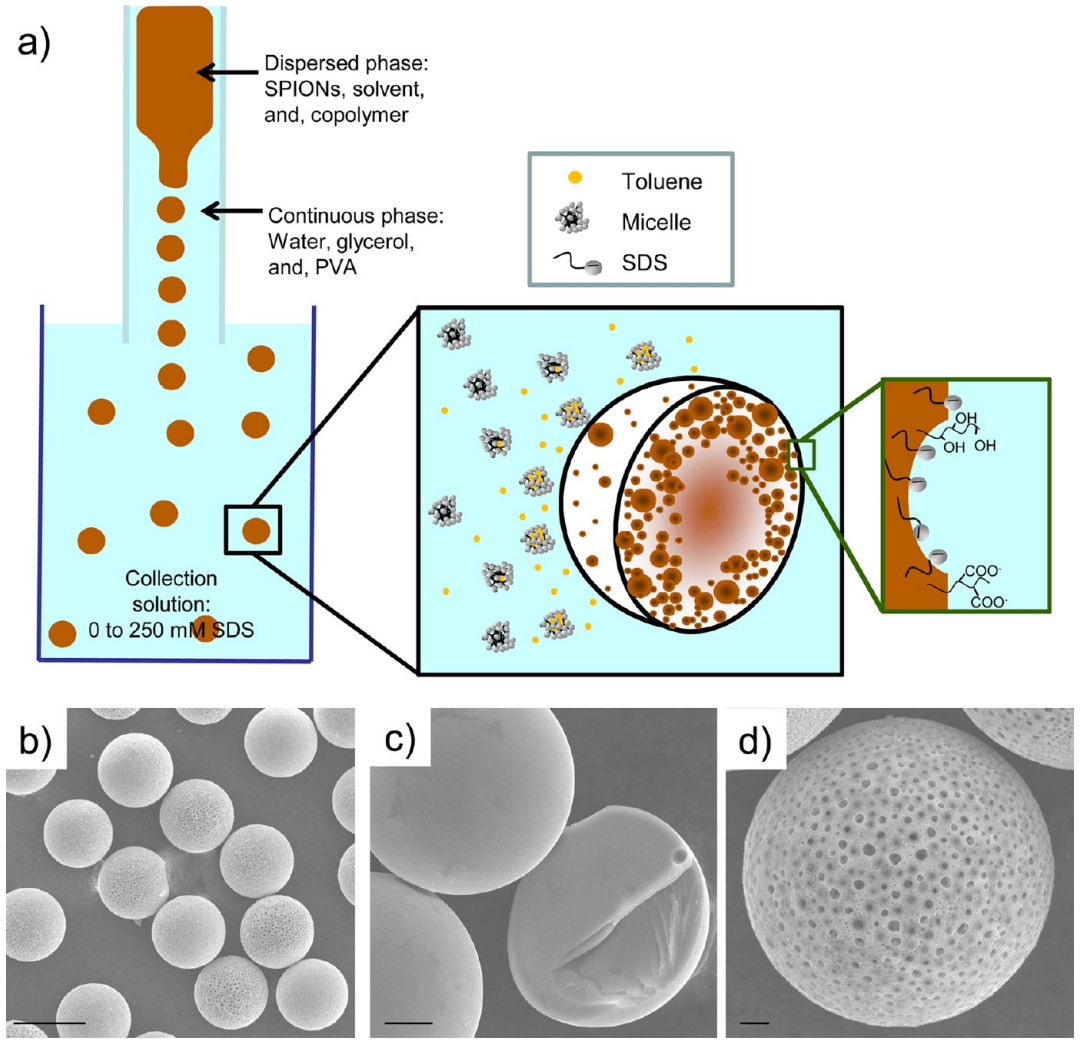

Figure 1. (a) Schematic of the generation of droplets and the formation of pores as solvent diffuses out of the droplet phase. The inset of the schematic shows that SDS, poly(vinyl alcohol) and hydrolyzed poly(styrene/maleic anhydride) are present at the surface of the droplet. (b) Low-magnification SEM images of microparticles (scale bar 100 μm). High-magnification SEM images of (c) nonporous microparticles and (d) porous microparticles (scale bars 10 μm).

Photopolymerization hardened the aqueous phase, yielding porous particles with porosity that could be controlled by adjusting the air and aqueous flow rates.

Using these approaches, the synthesis of microparticles containing a high loading of SPIONs was unsuccessful due to the strong absorption of light by the SPIONs which rendered photoinitiation inefficient. In response, we introduce herein a strategy that allows the fabrication of beads in a single step starting from SPIONs and a functional polymer yielding microparticles with a solid or porous internal structure. The method is based on the assembly of material and thus does not rely on any chemical transformation such as polymerization, cross-linking or sol−gel processes. We demonstrate this concept using superparamagnetic iron oxide nanoparticles (SPIONs), which have a strong absorption in the ultraviolet and visible wavelength range rendering mixtures containing it difficult to photopolymerize. By combining SPIONs with a functional polymer, we show how these materials can be assembled into functional magnetic microparticles with control over their size and porosity while maintaining narrow size distributions through judicious choice of solvent or by varying the concentration of surfactant in the collection solution.

2. EXPERIMENTAL SECTION

Materials. An alternating copolymer of poly(styrene/maleic anhydride) [75:25] (MW 9500 g/mol) and poly(vinyl alcohol) (MW 6000 g/mol) were purchased from Polysciences, Inc. Superparamagnetic iron oxide nanoparticles (SPIONs) with fatty acids ligands were purchased from Ferrotec. The Ferrotec SPIONs were analyzed by TEM to have a diameter of 9.1 ± 2.7 nm. Poly(styrene/maleic anhydride) was functionalized with Alexa Fluor594 Cadaverine from Invitrogen (400 mg) by reacting it with the copolymer (0.1 mg) in THF. The polymer was purified by precipitation in water and redispersion in THF. Glycerol, toluene, hexanes, and chloroform were all ACS grade reagents. Water filtered through a Millipore filtration system was used for all syntheses and experiments.

Fabrication of the Microfluidic Device. The design of the microcapillary device was based on the work by Utada et al. with the following modifications.[19] Briefly, a glass capillary with a luer tip attached to one end was heated and pulled to a desired diameter. A second capillary with an internal diameter of 500 μm was fitted with luer stub as a side arm. The tapered capillary was then inserted into the larger capillary fused by a ring seal. The continuous and dispersed phases were flown in the microfluidic devices driven by two KD Scientific syringe pumps. Droplets were generated with flow rates of 200 mL/h for the continuous phase and 0.5 mL/h for the dispersed phase unless stated otherwise.

Instrumentation. Scanning electron microscopy (SEM) images were acquired with a JEOL JSM840A at an accelarating voltage of 20 kV. Epifluorescence and brightfield images were taken using Olympus IX81 and BX51 microscopes. Fluorescence was excited with a 633 nm laser and detected via a Cy5 filter set (Chroma Technology) with a Cascade 512B EMCCD camera (Photometrics, US). For the N_2 isotherm measurements, the microsphere sample was oven-dried at 70 °C for 48 h. After transferring the sample into an analysis cell, it was outgased in the analysis port at room temperature (23 ± 1 °C) for 24 h. The N_2 isotherm was acquired at 77.3 K using ASAP 2010 porosimeter (Micromeritics, USA). Ultra high purity nitrogen gas (Praxair, Canada, 99.999% purity) was used.

The magnetic susceptibility measurements were conducted with a Quantum Design SQUID magnetometer MPMS-XL. This magnetometer works between 1.8 and 400 K for direct current (dc) applied fields ranging from −7 to 7 T. The magnetic data were corrected for the sample holder and the diamagnetic contributions.

3. RESULTS AND DISCUSSION

The microfluidic device used in this work was made from coaxially assembled capillaries. The tip of the inner capillary tapered to a diameter of approximately 100 μm while the internal diameter of the outer capillary was 500 μm. The dispersed phase consisted of SPIONs and the functional copolymer, poly(styrene/maleic anhydride) dissolved in organic solvent such as hexane, toluene, a toluene/tetrahydrofuran (THF) mixture, or chloroform. The dispersed phase was sheared into droplets by the flow of the continuous phase composed of glycerol (64 wt %), poly(vinyl alcohol) (2 wt %) and water (34 wt %). Droplets traveled for ∼2 s in the microfluidic device before being collected in an aqueous solution of sodium dodecyl sulfate in which the droplets formed microparticles with morphologies governed by the composition of the collection solutions and the solvent used in the dispersed phase.

The continuous phase was formulated with glycerol to impart the fluid with a high viscosity and thus generate higher shear forces at lower flow rates while the poly(vinyl alcohol) (PVA) acted as a good stabilizer for the droplets. Under these conditions, it was possible to suppress the coalescence of the droplets as they entered the collection solutions. Once the droplets were gathered from the channels into a collection solution, the solvent diffused out of the droplets into the aqueous phase. Results from thermogravimetric analysis and optical spectroscopy show that a fraction of the polymer is lost to the aqueous phase during the microparticle formation whereas no significant amount of SPION is found in the aqueous phase (see Figure SI_1 in the Supporting Information). Therefore, with their limited solubility in water, the SPIONs and copolymer remain in the droplet phase while the solvent diffuse out ultimately concentrating the droplet phase to form beads of densely packed nanoparticles and polymer. The schematic in Figure 1a depicts the generation of droplets in the microfluidic channels and the formation of pores that grow at the interface of the droplet toward the center of the droplet. The SEM images in Figure 1b−d showcase the range of particle morphology that form by mediating the rate of solvent removal and interfacial tension of the droplet.

The size of the particles could be tuned by varying the flow rates of the continuous or dispersed phase as predicted by droplet generation in the dripping mode. The size distribution of the droplets generally had a coefficient of variation (CV) of 2−3%. The beads maintained the same narrow size distribution if coalescence of the droplets was avoided or if the depletion of solvent occurred at a uniform rate. The addition of poly(vinyl alcohol) and the use of viscous glycerol helped to minimize coalescence, while gentle shaking of the beads after their collection ensure that the beads formed under uniform conditions. However, the size distribution of the microparticles generally increased to 2−8% CV. Figure 2 shows the decrease

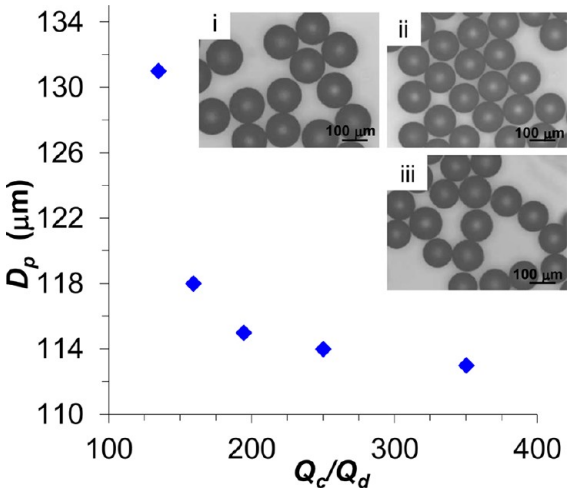

Figure 2. Diameter of microparticles formed as a function of the flow rate ratio of the continuous phase to the dispersed phase (Q_c/Q_d). The inset shows optical micrographs of the particles formed at Q_c/Q_d of (i) 135 , (ii) 195, and (iii) 350 .

in size of the microparticles with increasing flow ratios of the continuous phase to the dispersed phase. The inset of the figure show optical micrographs of the particles of various sizes and their narrow size distributions at three flow rate ratios.

Role of [SDS]. Droplets made from 150 mg/mL SPIONs and 5 mg/mL copolymer in toluene were generated in microfluidic channels and collected in 0 to 250 mM SDS solutions. After several hours of gentle mixing in the collection solution, the microparticles were magnetically purified and imaged by SEM. Images revealing the interior of the particles are found in Figure 3. The images show striking differences in morphology depending on the concentration of SDS of the collection solution, ranging from solid to porous interiors. More specifically, when [SDS] ≤ 10 mM, the microparticles are solid spheres of densely packed nanoparticles and polymer. On the other hand, particles prepared in [SDS] of 25 or 50 mM have large porous and open cellular structures, whereas those formed in [SDS] ≥ 100 mM have denser channellike structures.

To gain an understanding of how these various structures formed, optical micrographs of the droplets were recorded during their transformation from droplets to microparticles. From these images, the diameters of the droplets, D, were determined and plotted as a % of the initial droplet diameter, D_0. The results found in Figure 3f, show how the droplets decrease in size and level off after a time that depends on the concentration of SDS in the collection solution. The leveling of droplet size was taken as the point at which microparticles are formed. The microparticles formed in [SDS] ≤ 10 mM formed slowly, over several hours up to a day. Conversely, the particles formed in [SDS] of 25 and 50 mM form in two stages: initially, the droplet diameter decreases rapidly to approximately 85% of D_0 at which point the change in the size of the droplets lessened significantly. A similar trend is observed for the beads

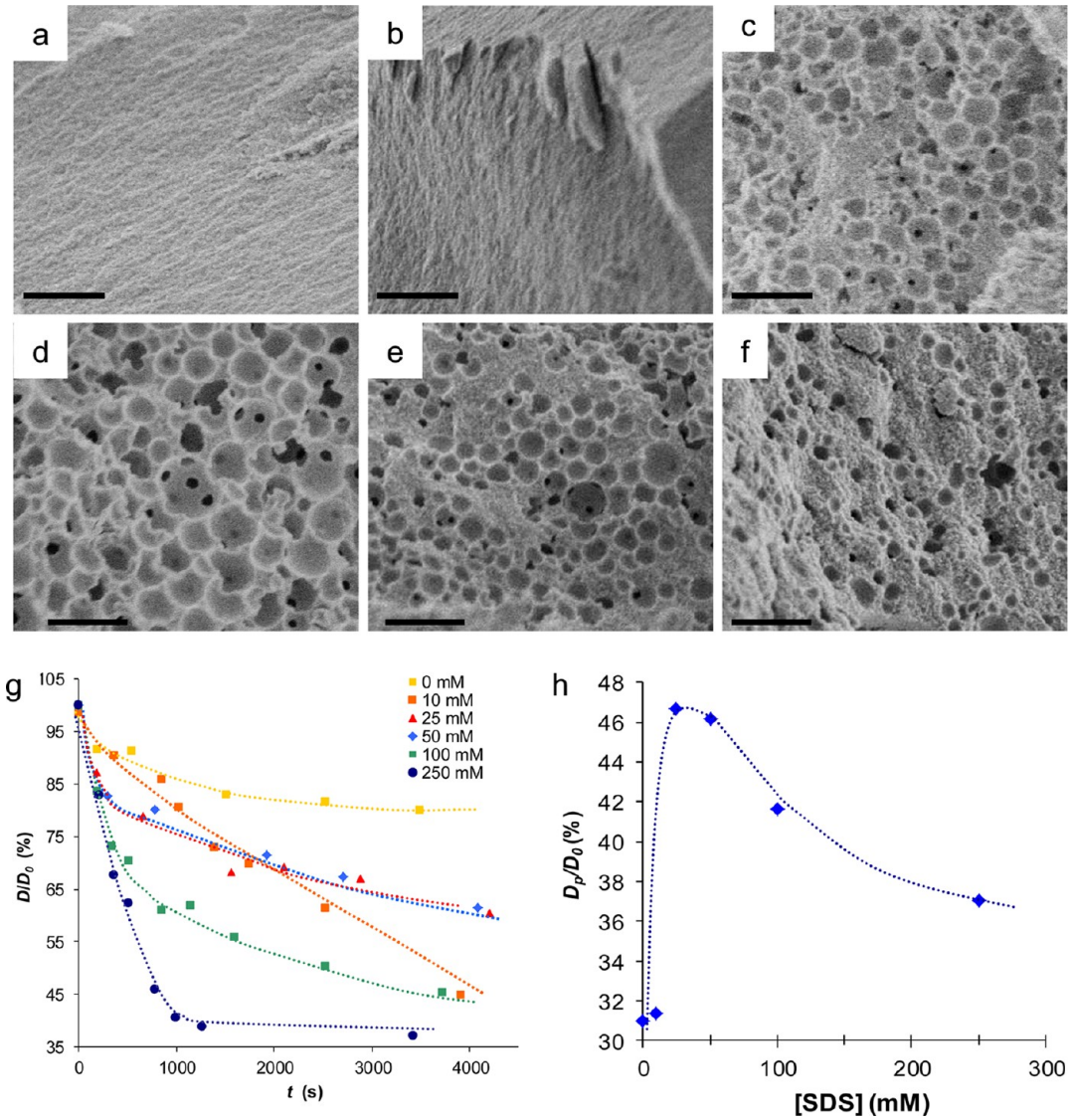

Figure 3. SEM images of the interior of the microspheres made from solutions of SPIONs and copolymer in toluene and collected in (a) 0, (b) 10, (c) 25, (d) 50, (e) 100, and (f) 250 mM SDS solutions (scale bar 1 μm), g) changes in droplet size as a function of time for droplets collected in various concentrations of SDS solutions. (h) Variation in the porosity of particles as a function of the concentration of SDS.

made in 100 mM SDS solutions; however, the transition in rates of change in the diameter occurred only after the droplets reached 75% of D_0. The particles collected in 250 mM SDS are formed from droplets that rapidly decrease in size to the final particle size.

The final diameter of the particles, D_p, expressed as a % of the initial droplet diameter is plotted as a function of [SDS] in Figure 3g. Since the droplets are formed from the same solutions, i.e. the SPION and copolymer solid content is constant in each droplet, then D_p/D_0 represents a measure of porosity. The porosities of the particles estimated from D_p/D_0 agree qualitatively with the SEM images. The porosity reaches a maximum when the particles are formed in intermediate concentrations of SDS, i.e. Twenty-five to 50 mM SDS. At [SDS] $\geq$100 mM, the porosity of the microparticles is lower, consistent with a more dense channel-like pores structure as observed in the SEM images. At [SDS] $\leq$ 10 mM, where D_p/D_0 is the lowest, the SEM images show no porosity. Moreover, the D_p/D_0 value of ~31% measured for particles formed in 0 and 10 mM SDS solutions compares well with a calculated value of 30% expected for nonporous particles based on the solid content of the dispersed phase and the density of the polymer and SPIONs.

These results demonstrate that SDS governs the formation of the microparticles and determines their final morphology. SDS can impact the conversion of droplet into microparticles in two ways. First, SDS forms micelles in the aqueous phase above the critical micelle concentration, CMC. Conductivity measurements on our SDS solutions indicate that the CMC is 8 mM (see Figure SI_2 in the Supporting Information). Although the CMC is likely to differ slightly in the presence of the droplets, glycerol and poly(vinyl alcohol), we can expect that near this concentration, a transition in rates of solvent depletion will occur. That is, the rate of transfer of toluene from the droplet phase to the aqueous phase will increase as the toluene present in the aqueous phase will relocate in the core of the micelle. Above the CMC, the concentration of micelles increases with increasing SDS and thus we can also expect a concurrent increase in the rates of solvent depletion from the droplets with increasing SDS concentration. Second, SDS can play a role in

the particle formation by acting as an amphiphile capable of adsorbing at the interface of the droplet and lowering the interfacial tension between the dispersed and continuous phase. Thus, at low concentration of SDS, i.e. 0−10 mM, the transport of toluene from the droplet to the aqueous phase is slow due to the absence of micelles. Toluene slowly diffuses out of the droplet phase into the aqueous phase driven by the finite solubility of toluene in water (0.57 g/L).[26] Furthermore, the concentration of surfactant is low enough that the expansion of the surface area of the droplet by the formation of pores is unfavorable. Therefore, the droplet shrinks without forming pores with the concentration of SPIONs and polymer gradually increasing until the droplet is drained of solvent and resulting in beads of densely packed SPIONs and polymer. As this process occurs slowly, the SPIONs can rearrange themselves inside the droplet to form a compact structure, as shown in the images of Figure 3a, b. The situation differs for particles formed in [SDS] of 25 and 50 mM. Here, the toluene can enter a micelle core once it has entered the aqueous phase, thereby pushing the equilibrium of toluene into the aqueous phase and increasing the rate of solvent depletion from the droplet. At these concentrations, there is also more surfactant available to stabilize the droplet interface. Therefore, concurrent with the diffusion of toluene from droplet to aqueous phase, SDS migrates to the droplet interface, stabilizing the surface and allowing the growth of pores. The SEM image of Figure 3c and d show the porous microparticle structure that result from preparing particles in these SDS solutions. We believe the transition in rates observed at 85% D_0 occurs when SDS is adsorbed at the interface which steadies the diffusion of toluene out of the droplet allowing sustained growth of the pores in parallel with slower solvent diffusion into the aqueous phase. A similar trend is observed with particles formed in 100 mM SDS except the transition occurs later, at ∼75% D_0. Therefore, more solvent is lost in the initial phase due to the increase in micelle concentration surrounding the droplet at this concentration. The second phase of particle formation, where the change in size slows, occurs when the droplet phase is more concentrated and thus more viscous. We speculate that the more viscous droplet phase may impede SDS adsorption as well as SPION mobility resulting in inefficient pore formation and a particle structure with lower porosity.

This mechanism of pore formation is supported by results comparing microparticles prepared in 100 mM SDS solution with those prepared in a solution containing 100 mM with 4.7 mM toluene added to it. The latter solution has micelle cores occupied by toluene and as a result once the droplets enter this solution, the rate at which toluene exits the droplet and enters the aqueous phase is lower. The slowed formation of particles was confirmed by measuring D/D_0 as a function of time, as shown in Figure 4a. These results show that the transformation of droplets into particles takes place over several more hours when the micelles are prefilled with toluene. Based on D_p/D_0, the porosity of the particles formed without and with toluene in the collection solution is 42 and 62%, respectively, in agreement with the SEM images found in Figure 4b−e that demonstrate the structure of the microparticles formed in toluene/SDS solutions are comparatively more porous than those formed in SDS solutions. Thus we show that particles with large open cellular structures can also develop by decreasing the rate of solvent diffusion into the aqueous phase using micelles prefilled with toluene and using high concentrations of surfactant.

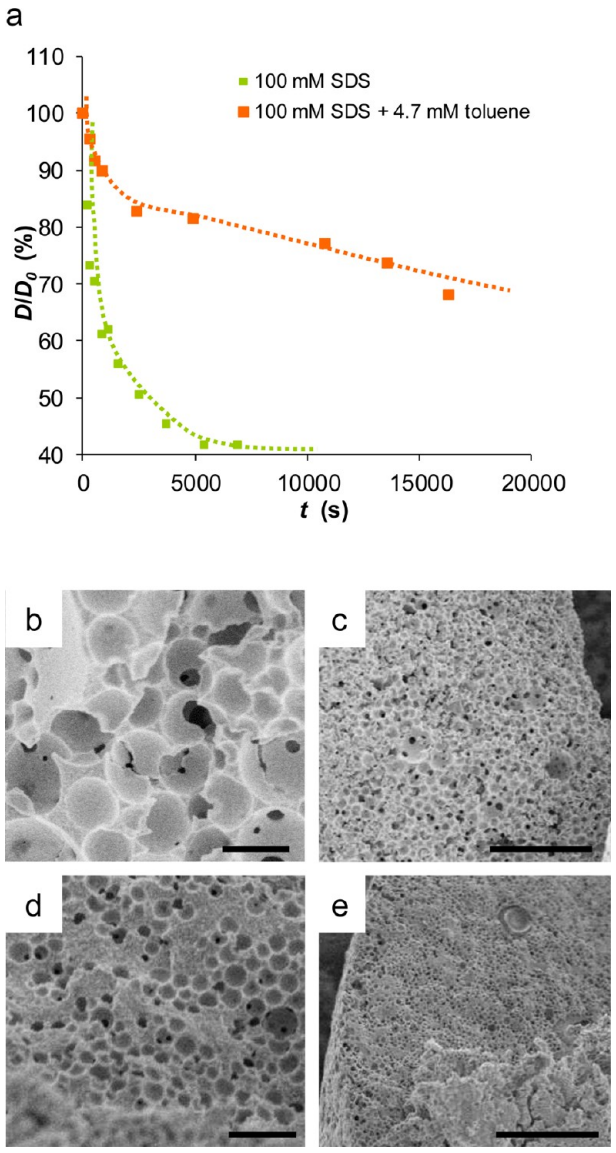

Figure 4. (a) Changes in droplet size as a function of time for droplets collected in solutions of 100 mM SDS and 100 mM SDS/4.7 mM toluene. SEM images of the interior of the microspheres formed in, (b, c) 100 mM SDS/4.7 mM toluene and (d, e) 100 mM SDS solutions. Scale bar 1 μm for b and d and 10 μm for c and e.

Role of the Solvent of the Dispersed Phase. The influence of the solvent used in the dispersed phase was investigated by producing microparticles starting from solutions of 150 mg/mL of SPION in chloroform, toluene, a mixture of THF and toluene (3:2), as well as hexane. In this series of particles, the copolymer was omitted because it is not soluble in hexane. The transformation of the droplets into microparticles was monitored by measuring D/D_0 at various times, as shown in Figure 5a. The results show that the droplets form particles after a few minutes for chloroform, about 1 h for toluene or the THF/toluene mixture and several hours when the dispersed phase is made from hexane. The time required for the particles to form follows the solubility of the solvent in water (chloroform, toluene, and hexane have solubilities in water of 8.1, 0.57, and 0.012 g/L, respectively, whereas THF is miscible in water).[26]

As shown in the SEM images of Figure 5b−e, these different rates impact the morphology of the particles. The micro-

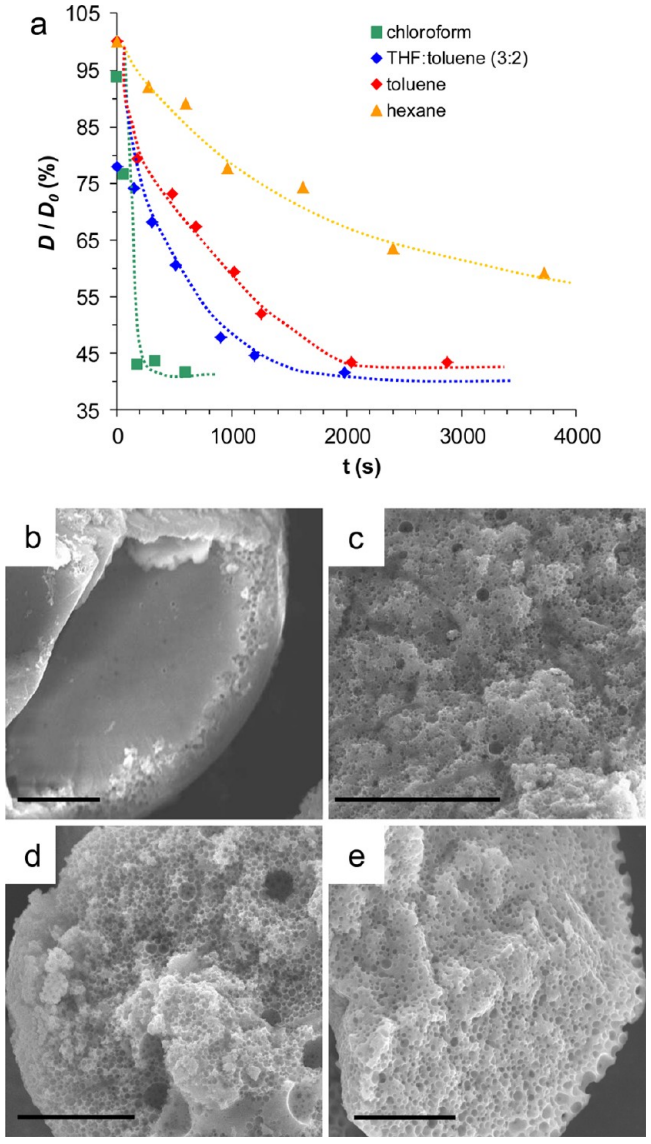

Figure 5. (a) Changes in droplet size as a function of time for droplets made from 150 mg/mL solutions of SPIONs in various solvents and collected in 100 mM SDS. SEM of the interior of particles formed from dispersed phases consisting of (b) chloroform, (c) a THF/toluene mixture (3:2), (d) toluene, and (e) hexane. Scale bar 10 μm.

particles formed from chloroform droplets have compact internal structures with a thin layer of pores at their surface. The morphology results from rapid removal of solvent from the droplets that prevents surfactant from stabilizing the surface and forming pores. The particles formed from a THF/toluene mixture show a dense porous structure. We speculate that this denser pore structure results from the mixing of water in the droplet phase due to the high content of water miscible THF. The increase in polarity of the droplet phase causes the SPIONs to precipitate, reducing the mobility of SPION in the droplet phase and causing inefficient adsorption of SDS at the interface that hinder pore formation. Conversely, the beads created from toluene droplets have macropores with a cellular structure, a result of the right balance between solvent removal, SDS adsorption, and, SPION solubility in the droplet phase (we note that these particles differ from the ones mentioned in the previous section by having no copolymer). The structure of the beads formed from hexane droplets has a more dense channellike structure. We observed that hexane was a poorer solvent for the SPIONs and thus we believe this morphology is also a result of lower solubility of the SPIONs in hexane which causes reduced SPION mobility and poor adsorption of SDS at the droplet interface. It is interesting to note that the large open pores at the surface of the particles give way to smaller more dense pores near the interior. This feature is likely the result of pore formation becoming progressively more inhibited as SPIONs are concentrated in the droplet and solvent is depleted.

Particle Characterization. To demonstrate how these microparticles could be functionalized, the copolymer poly(styrene/maleic anhydride) was reacted with the fluorescent dye Alexa Fluor594 Cadaverine (Invitrogen), prior to being used to form microparticles. Microparticles were prepared from a mixture containing 75 mg/mL of the dye-modified polymer and 100 mg/mL SPIONs in toluene. The droplets generated from this disperse phase were collected in 100 mM toluene. Fluorescent images of the purified microparticles are shown in Figure 6a. The images show the fluorescence of the polymer throughout the microparticles with brighter areas showing the pores. These results demonstrate it is possible to functionalize the polymer prior to preparing the particles. Alternatively, particles made from unreacted copolymer will form carboxylic acid groups when the maleic anhydride moiety reacts with the aqueous phase (water or the alcohol groups from glycerol or polyvinyl alcohol will ring open the anhydride to yield at minimum of one carboxylic acid group), which can subsequently be used for further particle functionalization.

Beads formed with 150 mg/mL SPION and 5 mg/mL copolymer in toluene and collected in 50 mM SDS solutions were analyzed by a magnetometer. Results, found in panels b and c in Figure 6, show that the microparticles have high

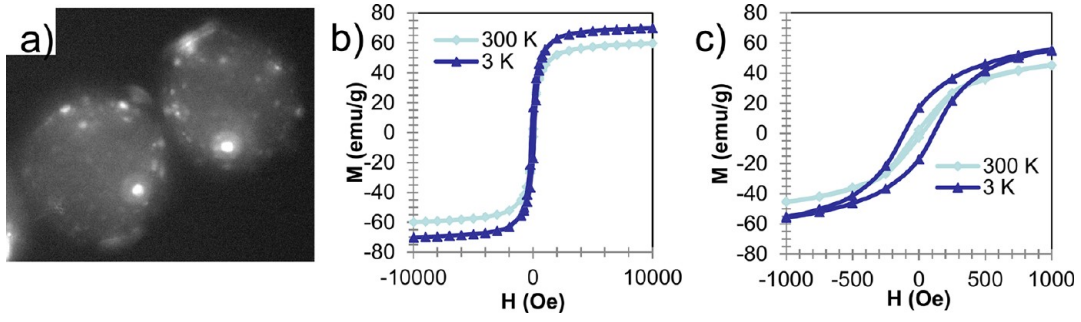

Figure 6. (a) Fluorescence image of porous microparticles formed from SPIONs and a dye-modified polymer. Mass magnetization curves at 3 and 300 K of porous beads at (b) high and (c) low fields.

dx.doi.org/10.1021/am301304h | ACS Appl. Mater. Interfaces 2012, 4, 4934−4941

saturation magnetizations of 61 emu/g. The high saturation magnetization of these particles, a result of the high concentrations of SPIONs, makes them valuable for use in applications that use weaker field gradients such as electromagnets. The magnetization curve of the microparticles shows near zero coercivity at 300 K, indicating that the microparticles preserve their superparamagnetic behavior after their assembly into particles.

Nitrogen isotherms measurements and BET calculations of the surface area were performed on microparticles formed in 25 mM SDS solution and with toluene used in the dispersed phase. The isotherm results are found in the Supporting Informations (Figure SI_3−SI_6). The isotherm showed type IIa character, a typical behavior for solid powders with a steep increase of the isotherm at $p/p_0 > 0.95$ indicating the presence of macropores (>50 nm). The very narrow hysteresis loop at $p/p_0 > 0.9$ shows that the sample lacks mesoporosity; the residual hysteresis loop can be possibly attributed to some aggregation (interparticle porosity) of the microspheres. The sample has some microporosity as determined by t-plot method. However, because no apparent steps at low relative pressures, $p/p_0 < 1 \times 10^{-2}$, can be observed in the $\log(p/p_0)$ plot of the isotherm, the apparent microporosity is likely due to surface heterogeneity. No apparent step is observed in the external monolayer formation region, $p/p_0 \approx 0.1$, which could indicate heterogeneity of adsorbent−adsorbate interactions. The t-plot transform appearance (higher slope in the plot below statistical thickness of 0.4 nm as compared with the slope at the higher statistical thickness limit) is consistent with weak adsorbent−adsorbate interactions. The total surface area of the microsphere sample was estimated by using a BET method. The BET transform showed linearity in the p/p_0 = 0.05−0.3 range yielding the BET total surface area (A_{BET}) of 5.2(1) m^2/g, of which external surface area (A_{ext}) is 4.2 m^2/g and micropore area (A_μ) of 1.0 m^2/g, as estimated using the t-plot method and a density of the beads of 4.3 g/cm^{-3}.

4. CONCLUSION

To conclude, different particle structures form as a result of an interplay between the rate of solvent depletion from the droplet, the adsorption of SDS at the droplet interface and the solubility of the SPIONs in the droplet phase. Figure 7 illustrates the various particle structures that result from using dispersed phases made up of solvent of different polarity and collection solutions of varying concentrations of SDS. Large open pores were formed at intermediate concentrations of SDS using toluene whereas microparticles with a denser pore structure were formed when hexane or a THF/toluene mixture was used in the dispersed phase. Solid particles on the other hand were generated only when the concentration of SDS of the collection solution was below 10 mM using either toluene or THF/toluene as the solvent in the disperse phase. This microfluidic approach to preparing magnetic non porous and porous macroparticles reported herein has the advantage of generating particles with control over size, porosity while maintaining narrow size distributions. Because the method is based on the assembly of materials, technically complicating processes such as photopolymerization is circumvented making this method ideal for preparing particles from materials that are sensitive to light and heat. The microparticles produced using this method do not form a surface skin and the pores are large interconnected, making them structures ideal for efficient flow of fluids.

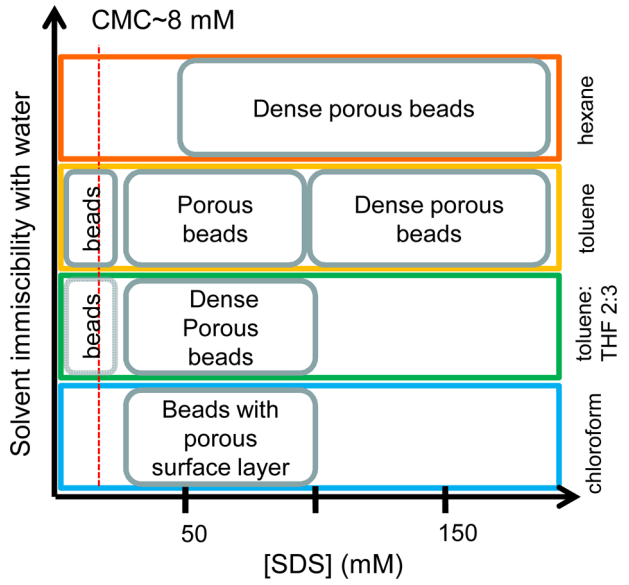

Figure 7. Graph showing the different microparticles that form using various solvents in the dispersed phase and concentrations of SDS as the collection solutions.

■ ASSOCIATED CONTENT

Ⓢ Supporting Information

Thermogravimetric analysis of particles; conductivity of SDS solutions; nitrogen isotherms. This material is available free of charge via the Internet at http://pubs.acs.org.

■ AUTHOR INFORMATION

Corresponding Author

*E-mail: chantal.paquet@nrc.ca.

Author Contributions

The manuscript was written through contributions of all authors. All authors have given approval to the final version of the manuscript.

Funding

This study was supported by CRTI−06−0187TD

Notes

The authors declare no competing financial interest.

■ ACKNOWLEDGMENTS

This study was supported by CRTI-06-0187TD We thank Muralee Murugesu for magnetometer measurements, Michael Vandenhoff for the microfluidic device and Gordon Chang for some SEM imaging.

■ REFERENCES

(1) Ye, C.; Chen, A.; Colombo, P.; Martinez, C. *J. R. Sci. Interface* **2010**, *7*, S461−S473.
(2) Prasad, N.; Perumal, J.; Choi, C.-H.; Lee, C.-S.; Kim, D.-P. *Adv. Funct. Mater.* **2009**, *19*, 1656−1662.
(3) Utada, A. S. *Science* **2005**, *308*, 537−541.
(4) Lorenceau, E.; Utada, A. S.; Link, D. R.; Cristobal, G.; Joanicot, M.; Weitz, D. A. *Langmuir* **2005**, *21*, 9183−9186.
(5) Nie, Z.; Li, W.; Seo, M.; Xu, S.; Kumacheva, E. *J. Am. Chem. Soc.* **2006**, *128*, 9408−9412.
(6) Xu, S.; Nie, Z.; Seo, M.; Lewis, P.; Kumacheva, E.; Stone, H. A.; Garstecki, P.; Weibel, D. B.; Gitlin, I.; Whitesides, G. M. *Angew. Chem., Int. Ed.* **2005**, *44*, 724−728.
(7) Chu, L.-Y.; Utada, A. S.; Shah, R. K.; Kim, J.-W.; Weitz, D. A. *Angew. Chem., Int. Ed.* **2007**, *46*, 8970−8974.

(8) Wang, J.-T.; Wang, J.; Han, J.-J. *Small* **2011**, *7*, 1728−1754.
(9) Kim, S.-H.; Won Shim, J.; Lim, J.-M.; Yeon Lee, S.; Yang, S.-M. *New J. Phys.* **2009**, *11*, 075014.
(10) Utada, A.; Fernandez-Nieves, A.; Stone, H.; Weitz, D. *Phys. Rev. Lett.* **2007**, *99*, 094502.
(11) Jeong, S.; Woo, K.; Kim, D.; Lim, S.; Kim, J. S.; Shin, H.; Xia, Y.; Moon, J. *Adv. Funct. Mater.* **2008**, *18*, 679−686.
(12) Seiffert, S.; Dubbert, J.; Richtering, W.; Weitz, D. A. *Lab Chip* **2011**, *11*, 966−968.
(13) Seo, M.; Nie, Z.; Xu, S.; Mok, M.; Lewis, P. C.; Graham, R.; Kumacheva, E. *Langmuir* **2005**, *21*, 11614−11622.
(14) Yuan, Z.-Y.; Su, B.-L. *J. Mater. Chem.* **2006**, *16*, 663−677.
(15) Gokmen, M. T.; Du Prez, F. E. *Prog. Polym. Sci.* **2012**, *37*, 365−405.
(16) Gijs, M. A. M.; Lacharme, F.; Lehmann, U. *Chem. Rev.* **2010**, *110*, 1518−1563.
(17) Wang, X.; Ding, X.; Zheng, Z.; Hu, X.; Cheng, X.; Peng, Y. *Macromol. Rapid Commun.* **2006**, *27*, 1180−1184.
(18) Chen, C.-H.; Abate, A. R.; Lee, D.; Terentjev, E. M.; Weitz, D. A. *Adv. Mater.* **2009**, *21*, 3201−3204.
(19) Pamme, N.; Eijkel, J. C. T.; Manz, A. *J. Magn. Magn. Mater.* **2006**, *307*, 237−244.
(20) Gong, X.; Wen, W.; Sheng, P. *Langmuir* **2009**, *25*, 7072−7077.
(21) Dubinsky, S.; Zhang, H.; Nie, Z.; Gourevich, I.; Voicu, D.; Deetz, M.; Kumacheva, E. *Macromolecules* **2008**, *41*, 3555−3561.
(22) Dubinsky, S.; Park, J.; Gourevich, I.; Chan, C.; Deetz, M.; Kumacheva, E. *Macromolecules* **2009**, *42*, 1990−1994.
(23) Zhang, H.; Ju, X.-J.; Xie, R.; Cheng, C.-J.; Ren, P.-W.; Chu, L.-Y. *J. Colloid Interface Sci.* **2009**, *336*, 235−243.
(24) Gokmen, M. T.; Van Camp, W.; Colver, P. J.; Bon, S. A. F.; Du Prez, F. E. *Macromolecules* **2009**, *42*, 9289−9294.
(25) Wan, J.; Bick, A.; Sullivan, M.; Stone, H. A. *Adv. Mater.* **2008**, *20*, 3314−3318.
(26) Abraham, M. H.; Le, J. *J. Pharm. Sci.* **1999**, *88*, 868−880.